星形成ゼミ
SF newsletter 342
#1 - #6

川邊

2020年7月2日

担当論文

1. **Observability of the Vertical Shear Instability in protoplanetary disk CO kinematics**
   Marcelo Barraza-Alfaro, Mario Flock, Sebastian Marino, Sebastián Pérez ★ Context. Dynamical and turbulent

2. **A major asymmetric ice trap in a planet-forming disk: II. prominent SO and SO2 pointing to C/O < 1**
   A. S. Booth, N. van der Marel, M. Leemker, E. F. van Dishoeck, S. Ohashi ★ Gas-phase sulphur bearing volatiles

3. **Zooming into the Collimation Zone in a Massive Protostellar Jet**
   Carlos Carrasco-González, Alberto Sanna, Adriana Rodríguez-Kamenetzky, Luca Moscadelli, Melvin Hoare,

4. **Constraining Spatial Densities of Early Ice Formation in Small Dense Molecular Cores from Extinction Maps**
   Laurie E. U. Chu, Klaus W. Hodapp ★ Tracing dust in small dense molecular cores is a powerful tool to study the

5. **TRAO Survey of the nearby filamentary molecular clouds, the universal nursery of stars (TRAO FUNS). II. Filaments and Dense cores in IC 5146**
   Eun Jung Chung, Chang Won Lee, Shinyoung Kim, Maheswar Gopinathan, Mario Tafalla, Paola Caselli, Philip

6. **Probing jets from young embedded sources: clues from HST near-IR [Fe II] images**
   Jessica Erkal, Brunella Nisini, Deirdre Coffey, Francesca Bacciotti, Patrick Hartigan, Simone Antoniucci, Teres

1. Observability of the Vertical Shear Instability in protoplanetary disk CO kinematics

Marcelo Barraza-Alfaro, Mario Flock, Sebastian Marino, Sebastián Pérez ★ Context. Dynamical and turbulent

Context. Dynamical and turbulent motions of gas in a protoplanetary disk are crucial for their evolution and are thought to affect planet formation. Recent (sub-)millimeter observations show evidence of weak turbulence in the disk's outer regions. However, the detailed physical mechanism of turbulence in these outer regions remains uncertain. The vertical shear instability (VSI) is a promising candidate mechanism to produce turbulence in the outer parts of the disk.
Aims. Our objective is to study the observability of the gas velocity structure produced by the vertical shear instability via CO kinematics with ALMA.
Methods. We perform global 3D hydrodynamical simulations of an inviscid and locally isothermal VSI-unstable disk. We post-process the simulation results with radiative transfer calculations, and produce synthetic predictions of CO rotational emission lines. Following, we compute the line of sight velocity map, and its deviations from a sub-Keplerian equilibrium solution. We explore the detectability of the VSI by identifying kinematic signatures using realistic simulated observations using the CASA package.
Results. Our 3D hydrodynamical simulations of the VSI show the steady state dynamics of the gas in great detail. From the velocity structure we infer a turbulent stress value of $\alpha_{r\phi} = 1.4 \times 10^{-4}$. On large scales, we observe clear velocity deviations in the order of 50 m s^{-1} as axisymmetric rings with radially interspersed signs. By comparing synthetic observations at different inclinations we find optimal conditions at $i \lesssim 20°$ to trace for the kinematic structures of the VSI. We found that current diagnostics to constrain gas turbulence from non-thermal broadening of the molecular line emission are not applicable to anisotropic VSI turbulence.
Conclusions. We conclude that the detection of kinematic signatures produced by the vertical shear instability is possible with ALMA's current capabilities. Observations including an extended antenna configuration are required to resolve the structure (beam sizes below ~ 10 au). The highest spectral resolution available is needed (~ 0.05 km s^{-1} with ALMA Band 6) for robust detection. The characterization of the large-scale velocity perturbations is required to constrain the turbulence level produced by the VSI from gas observations.

PPD(特に、MRI-Magneto-Rotational-Instability-の働かない MRI "dead-zone"の外縁部)
　における乱流の起源と考えらるVSI (Vertical Shear Instability)の観測可能性を調べた。
方法は3D 流体計算 : 非粘性、局所的にisothermalで VSI 不安定円盤を仮定
計算結果を輻射輸送計算(CO輝線) を用いて、VSIの検出可能性を調べるため
　CASAでの擬似観測を行った　　Stress-to-pressure ratio
結果 : simulationで、詳細なgasの定常運動を描き出した　(=> turbulent stress value~10^{-4})
　　動径方向に、速度場で~50 m/sの偏りが現れる(軸対称構造が、繰り返し現れる)
　　i< 20 deg.が観測に optimal で、ALMAでは10 au以下と、0.05 km/sの分解能が必要

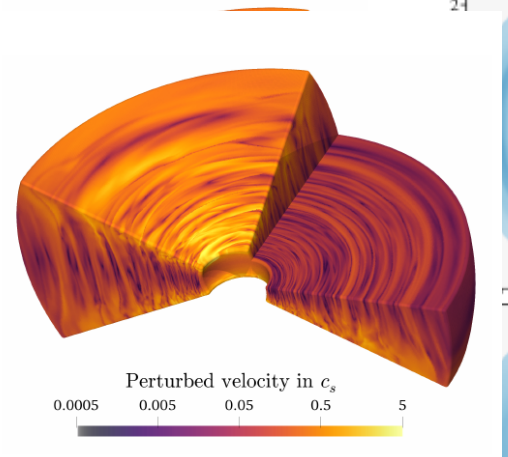

Fig. 2. 3D rendering of a VSI-unstable protoplanetary disk. The color map shows the perturbed total velocity of the gas in units of the local sound speed. Only half of our simulation domain in azimuth is shown for visualization purposes.

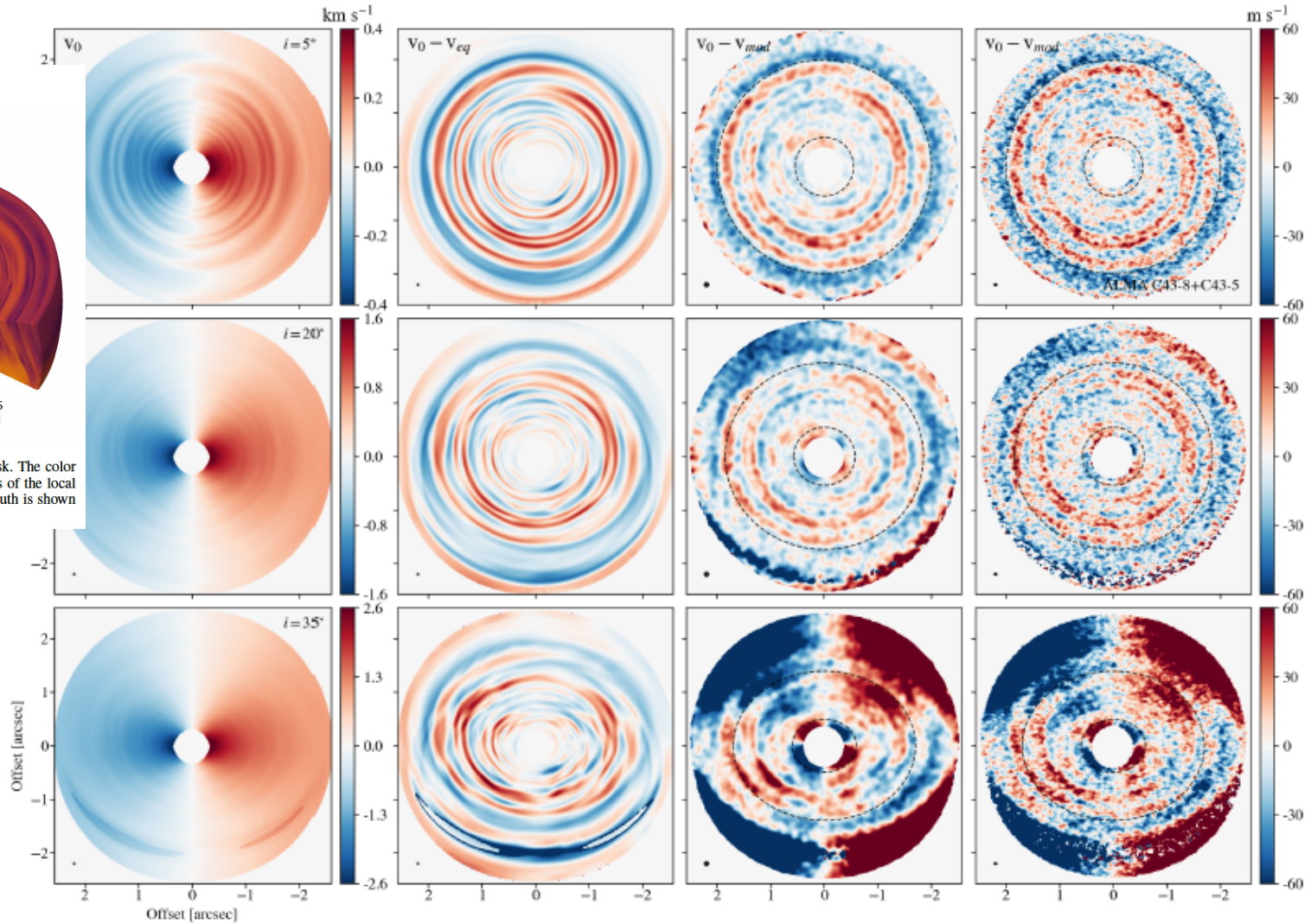

Fig. 4. Results of the line of sight velocity map and extracted velocity perturbations from a VSI unstable disk ^{12}CO(2-1) synthetic lines observations. The velocity centroid of the line was computed at each pixel from mock data cubes with a velocity resolution of 0.05 km s^{-1}. The input fields are shown in Figure 3, which corresponds to a disk after ∼ 0.3 Myr of evolution. From top to bottom, are shown the results for disk inclinations of 5°, 20° and 35°. *First column:* Velocity centroid maps (v_0). The images are convolved by a circular Gaussian beam of 50 mas and have no noise. *Second column:* Residual map of subtracting to v_0 the velocity centroid map obtained from a disk following an equilibrium solution (v_{eq}). *Third column:* Residual of subtracting to v_0 the best fit disk model obtained using EDDY (v_{mod}). The model corresponds to a geometrically thick disk that follows power-law profiles for the velocities in the radial and azimuthal directions. The images in this case are convolved by a 0.1 arcsecond circular Gaussian beam and have an RMS noise of ∼ 1.5 mJy beam^{-1}. *Fourth column:* The same as the third column, but for a 20 h Cycle 7 ALMA simulated observation using configurations C43-8 and C43-5, with an RMS noise of ∼ 1.5 mJy beam^{-1}. The resulting beam size of our synthetic

2. **A major asymmetric ice trap in a planet-forming disk: II. prominent SO and SO2 pointing to C/O < 1**

A. S. Booth, N. van der Marel, M. Leemker, E. F. van Dishoeck, S. Ohashi

★ Gas-phase sulphur bearing volatiles appear to be severely depleted in protoplanetary disks. The detection of CS and non-detections of SO and SO2 in many disks have shown that the gas in the warm molecular layer, where giant planets accrete their atmospheres, has a high C/O ratio. In this letter, we report the detection of SO and SO2 in the Oph-IRS 48 disk using ALMA. This is the first case of prominent SO2 emission detected from a protoplanetary disk. The molecular emissions of both molecules is spatially correlated with the asymmetric dust trap. We propose that this is due to the sublimation of ices at the edge of the dust cavity and that the bulk of the ice reservoir is coincident with the millimetre dust grains. Depending on the partition of elemental sulphur between refractory and volatile materials the observed molecules can account for 15-100% of the total sulphur budget in the disk. In strong contrast to previous results, we constrain the C/O ratio from the CS/SO ratio to be < 1 and potentially solar. This has important implications for the elemental composition of planets forming within the cavities of warm transition disks.

PPDでは、Gas-phaseのS-bearing 揮発成分は、非常に少ないと考えられる:
　多くのPPDでは、CSは検出、SO SO2は未検出で、ガス惑星大気は高いC/O比が期待
今回、Oph-IRS 48 diskで、SO, SO2をALMAで検出: 強いSO2が検出されたのは最初の例
Dusty cavityのinner edgeでの氷の昇華が、SO, SO2のが起源と考えられる
(or 昇華したH2SとH2Oの気相反応で生成)
揮発成分と非揮発性分(refractory)にどのようにSが含まれているかにも寄るが、
　観測で検出されたSO, SO2は、S全体の15-100 %に相当
これまでの観測結果とは対照的に、C/O < 1でsolar (i.e., C/O ~ 0.4) の可能性あり。
暖かい遷移円盤内で形成される惑星の組成に影響を与える可能性

Oph-IRS 48:
Band7 観測

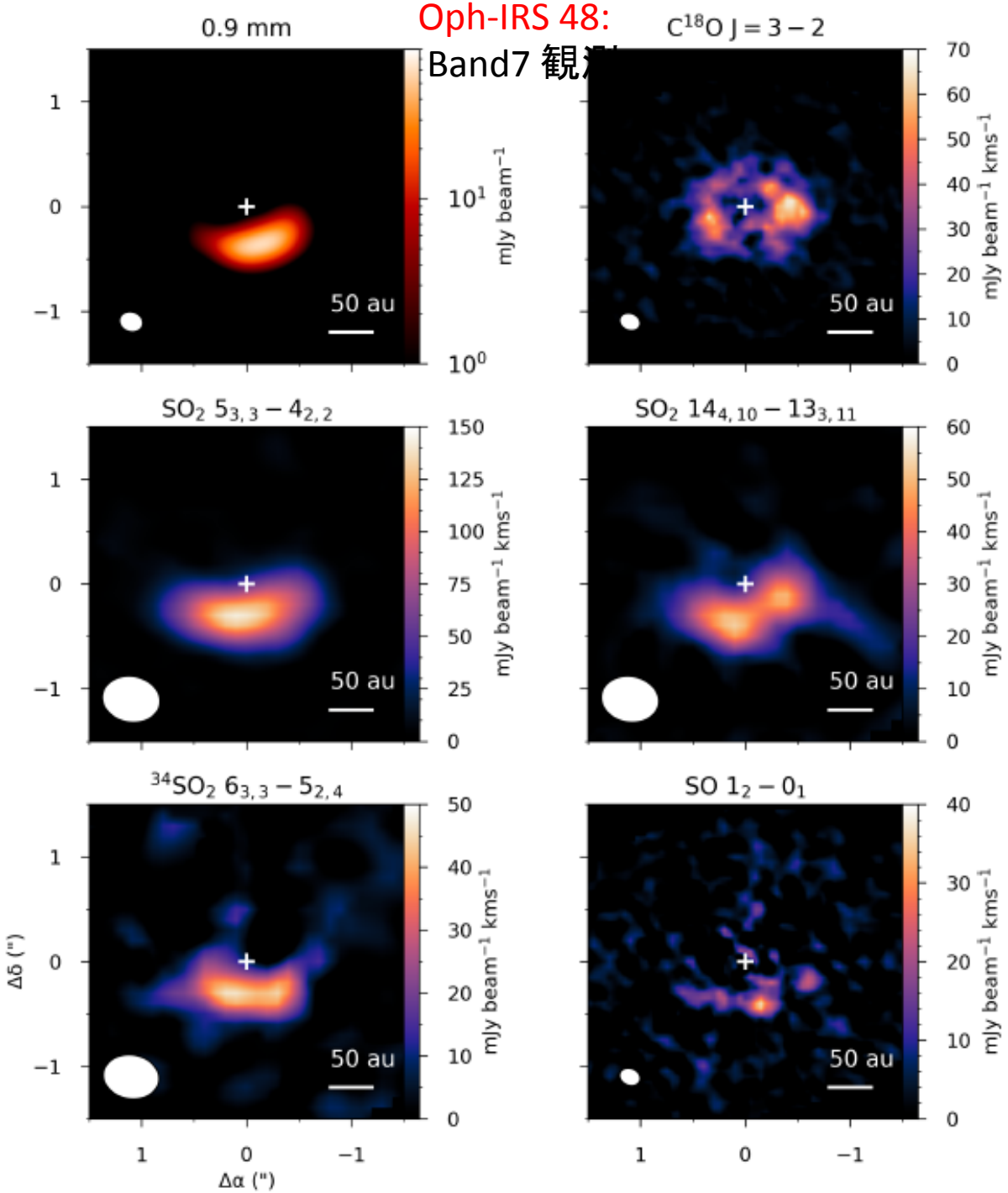

Table 2. Derived column densities and ratios

Molecule	T_{ex} (K)	N_T (cm^{-2})	τ
SO_2*	50	$2.6 \pm 0.3 \times 10^{15}$	[> 1]
	100	$4.4 \pm 0.4 \times 10^{15}$	[> 1]
	150	$6.6 \pm 0.4 \times 10^{15}$	[> 1]
$^{34}SO_2$	50	$1.2 \pm 0.1 \times 10^{14}$	[0.26]
	100	$2.0 \pm 0.2 \times 10^{14}$	[0.08]
	150	$3.0 \pm 0.3 \times 10^{14}$	[0.04]
SO	50	$4.7 \pm 0.5 \times 10^{15}$	[0.60]
	100	$7.1 \pm 0.7 \times 10^{15}$	[0.16]
	150	$9.9 \pm 1.0 \times 10^{15}$	[0.08]
CS	50	$\leq 5.9 \pm 0.6 \times 10^{13}$	[≤2.3]
	100	$\leq 2.9 \pm 0.3 \times 10^{13}$	[≤0.35]
	150	$\leq 3.2 \pm 0.3 \times 10^{13}$	[≤0.14]
S/H	50	4.6×10^{-7}	-
	100	7.2×10^{-7}	-
	150	1.0×10^{-6}	-
CS/SO	50	≤0.012	-
	100	≤0.004	-
	150	≤0.003	-
SO/SO_2	50	1.8	-
	100	1.6	-
	150	1.5	-

* using $^{34}SO_2$ and $^{32}S/^{34}S = 22$

3. Zooming into the Collimation Zone in a Massive Protostellar Jet

Carlos Carrasco-González, Alberto Sanna, Adriana Rodríguez-Kamenetzky, Luca Moscadelli, Melvin Hoare, José M. Torrelles, Roberto Galván-Madrid, Andrés F. Izquierdo ★ Protostellar jets have a fundamental role at the earliest evolution of protostars of all masses. In the case of low-mass (<8 Msun) protostars, strong observational evidence exists that the launching and collimation is due to the X- and/or disk-wind mechanisms. In these models, it is the protostar/disk system that creates all the necessary conditions to launch and collimate the jets near the protostar via strong magnetic fields. The origin of jets from more massive protostars has been investigated much less, in part because of the difficulty of resolving the collimation zone in these more distant objects. Here we present the highest angular resolution observations of a jet powered by a massive protostar, the Cep A HW2 radio jet. We imaged the radio emission at projected distances of only 20 au from the protostar, resolving the innermost 100 au of a massive protostellar jet for the first time. The morphology of the radio jet emission in this massive object is very different than what is usually observed in jets from low-mass protostars. We found that the outflowing material in HW2 has two components: a wide-angle wind launched from the protostar/disk system, and a highly collimated jet starting at 20-30 au from the protostar. We discuss two possible scenarios: an extension of the classical disk-wind to a massive protostar, or external collimation of a wide-angle wind. These results have important consequences for our understanding of how stars of different masses are formed.

Low mass starにおけるradio jet形成の理論的な理解に比べて、high-massの場合は未解明
Massive (B-type) Protostar Cep A HW2 の radio jetを詳細に観測: JVLA 3.6 cm他 & 20 au
Protostarから100au領域のjetの構造を初めて観測:
20 au領域からのwide-angle wind と highly-collimated jetを見出した
2つの形成モデルを考察
1) classical disk wind model
2) external collimation of wide-angle wind

VLA
3.6 cm ＆ 1.3 cm

白コンター
NOEMA 1.3mm
(disk)

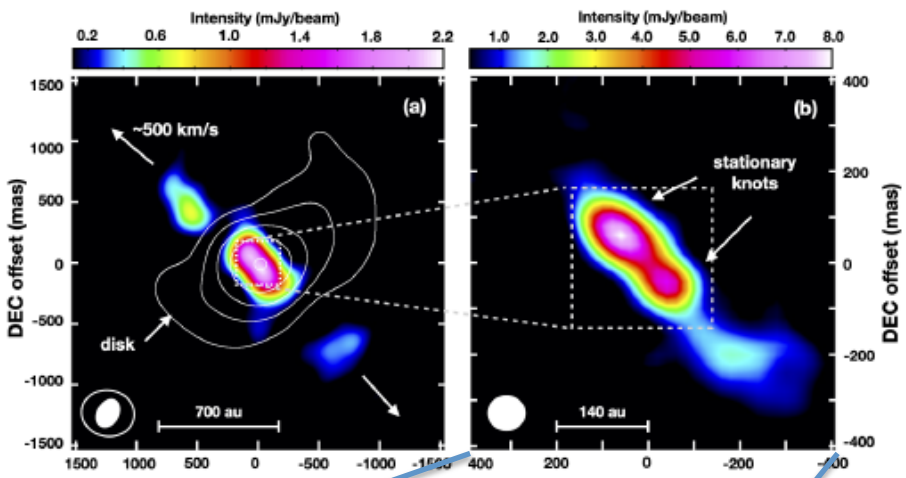

VLA
7.5mm
(40GHz)

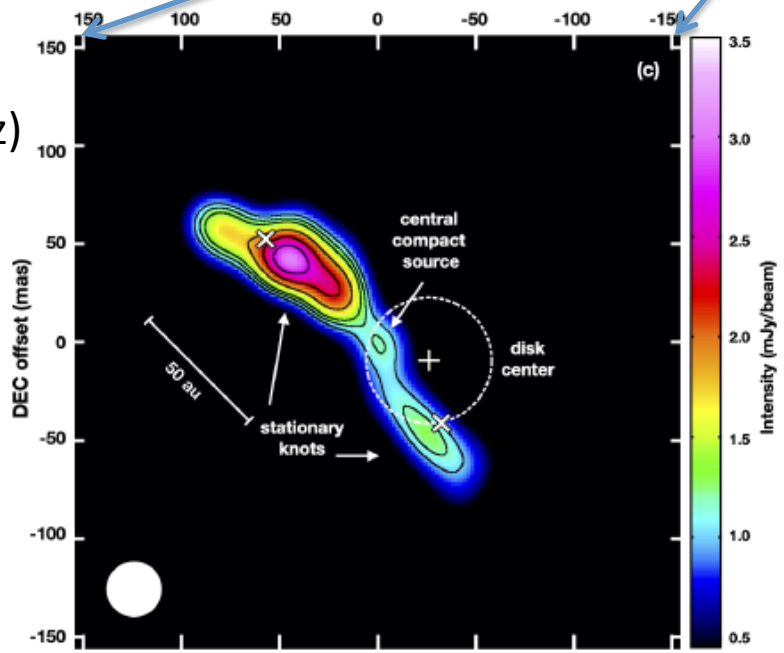

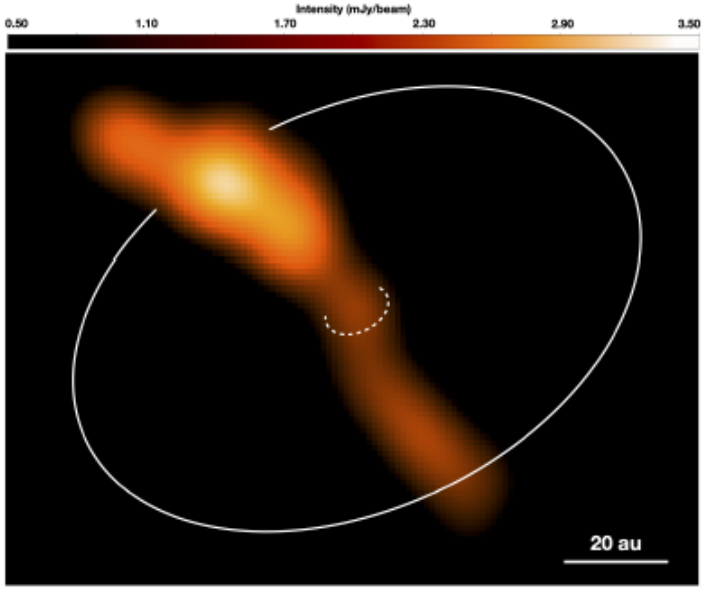

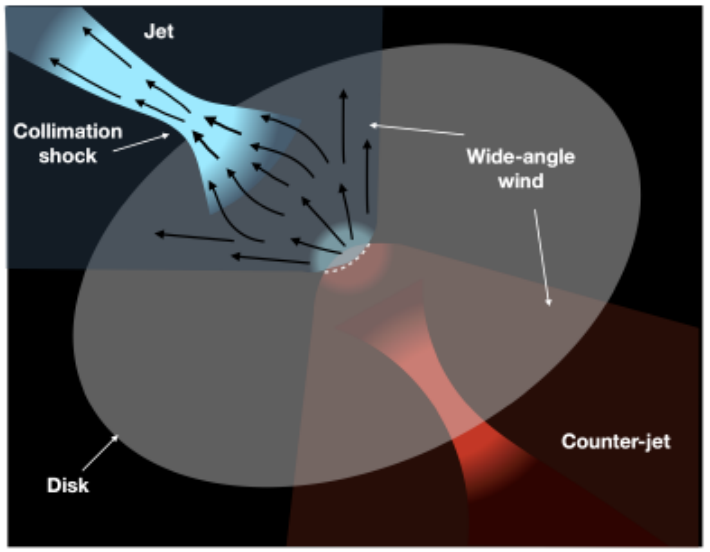

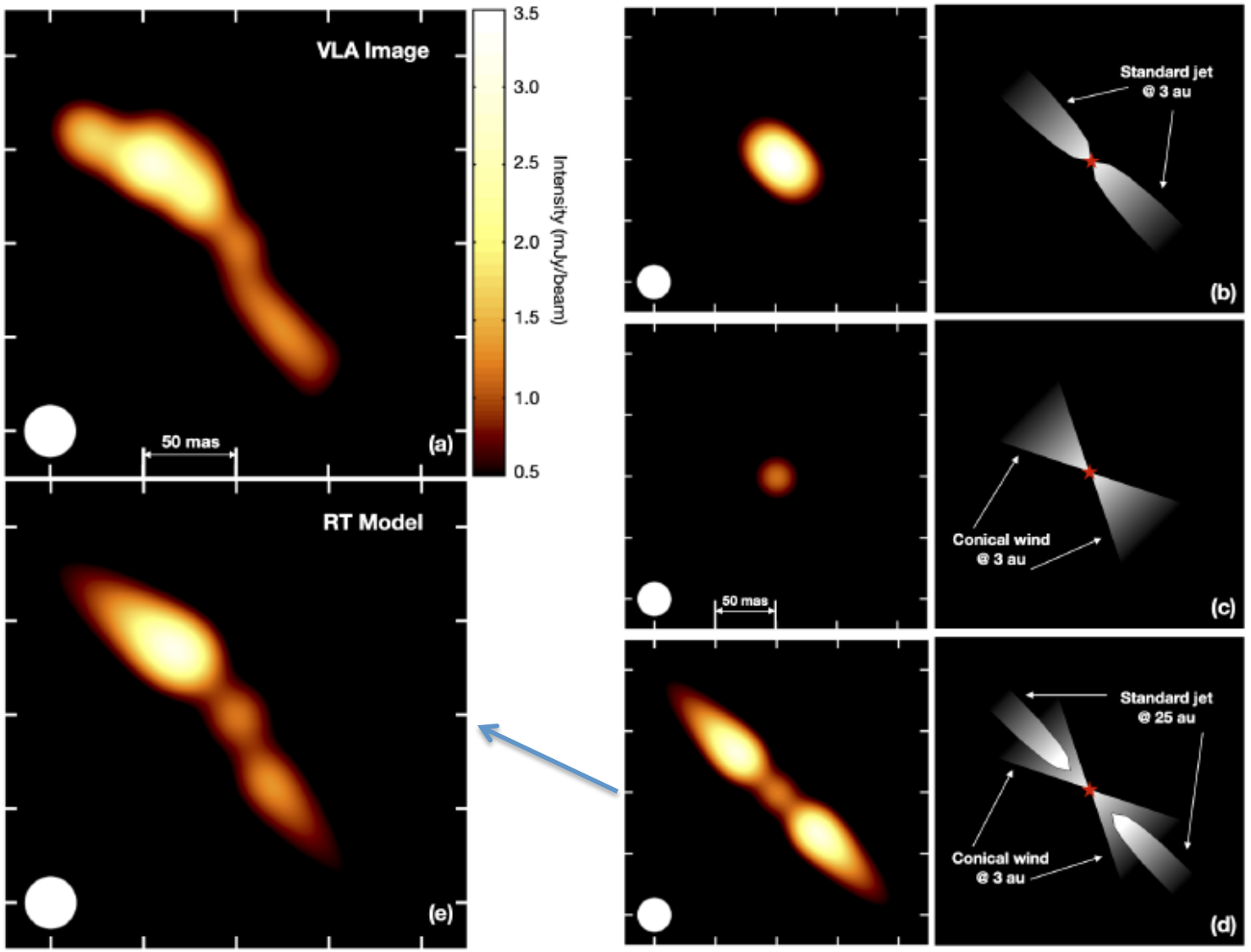

Figure 2. A radiative transfer modeling of the 7.5 mm image of Cep A HW2. **(a)** Image of the radio jet as shown in Figure 1c. **(b)** A model consisting of a standard jet (Reynolds 1986) starting at 3 au from the protostar. The left panel is the output image from the radiative transfer model with the same intensity scale of panel (a); the right panel shows a schematic view of the jet. As can be seen, an elongated bright source is expected. **(c)** Same as (b) for a conical wind starting at 3 au from the protostar. The output image only shows a compact source which traces the densest part of the wind. **(d)** A combination of a conical wind starting at 3 au, and a standard jet starting at 25 au from the protostar. **(e)** Same as panel (d) but the north and south parts of the jet have slightly different P.A.s and mass-loss rates.

4. **Constraining Spatial Densities of Early Ice Formation in Small Dense Molecular Cores from Extinction Maps**

Laurie E. U. Chu, Klaus W. Hodapp ★

Tracing dust in small dense molecular cores is a powerful tool to study the conditions required for ices to form during the pre-stellar phase. To study these environments, five molecular cores were observed: three with ongoing low-mass star formation (B59, B335, and L483) and two starless collapsing cores (L63 and L694-2). Deep images were taken in the infrared JHK bands with the United Kingdom Infrared Telescope (UKIRT) WFCAM (Wide Field Camera) instrument and IRAC channels 1 and 2 on the Spitzer Space Telescope. These five photometric bands were used to calculate extinction along the line of sight toward background stars. After smoothing the data, we produced high spatial resolution extinction maps (~13-29") . The maps were then projected into the third dimension using the AVIATOR algorithm implementing the inverse Abel transform. The volume densities of the total hydrogen were measured along lines of sight where ices (H_2O, CO, and CH_3OH) have previously been detected. We find that lines of sight with pure CH_3OH or a mixture of CH_3OH with CO have maximum volume densities above 1.0×10^5 cm^{-3}. These densities are only reached within a small fraction of each of the cores (~0.3-2.1%). CH_3OH presence may indicate the onset of complex organic molecule formation within dense cores and thus we can constrain the region where this onset can begin. The maximum volume densities toward star-forming cores in our sample ($\sim1.2\text{-}1.7\times10^6$ cm^{-3}) are higher than those toward starless cores ($\sim3.5\text{-}9.5\times10^5$ cm^{-3}).

星形成以前に様々なicesの形成に制限を与える上で、高密度コアでのダスト定量は大事な方法

JHK and IRAC 3.6, 4.6 umのDeep imaging => background stars を使ってextinction maps

観測対象：3つの低質量星形成コア(B59, B335, L438) と 星無しコア(L63, L694)

“AVIATOR” algorithm(逆Abel変換)で、3次元分布(Hydrogen volume density)に変換

Ices (H2O: 3.0 um, CO: 4.67 um, CH3OH: C-H stretching mode 3.53 um) absorption features が検出されているコア(Chu+2020)で、Hydrogen volume densityを求めた

=> CH3OH or CH3OH/CO mixture のところでは、> 1.0 x 10^5 cm^{-3} (各コアの~ 0.3-2.1 %)

=> star forming coreのmax. density ~ (1.2 -1.7) x 10^6 cm^{-3}

max (starless) ~ (3.5 – 9.5) x 10^5 cm^{-3}よりも大きい

Chu+ 2020:
Observations of the Onset of Complex Organic Molecule Formation in Interstellar Ices

(同じ著者による先行研究)

-Cloud Core付随のYSOs
-背景星
-その他YSOs
方向で H2O, CO, CH3OH Iceの吸収線探査

Prestellar cores で CH3OH, CO ice が共に見つかった

⇒ CO => CH3OHへの変換が進んでいる。
(COはgas phaseに多い、CH3OHはice dominate?)

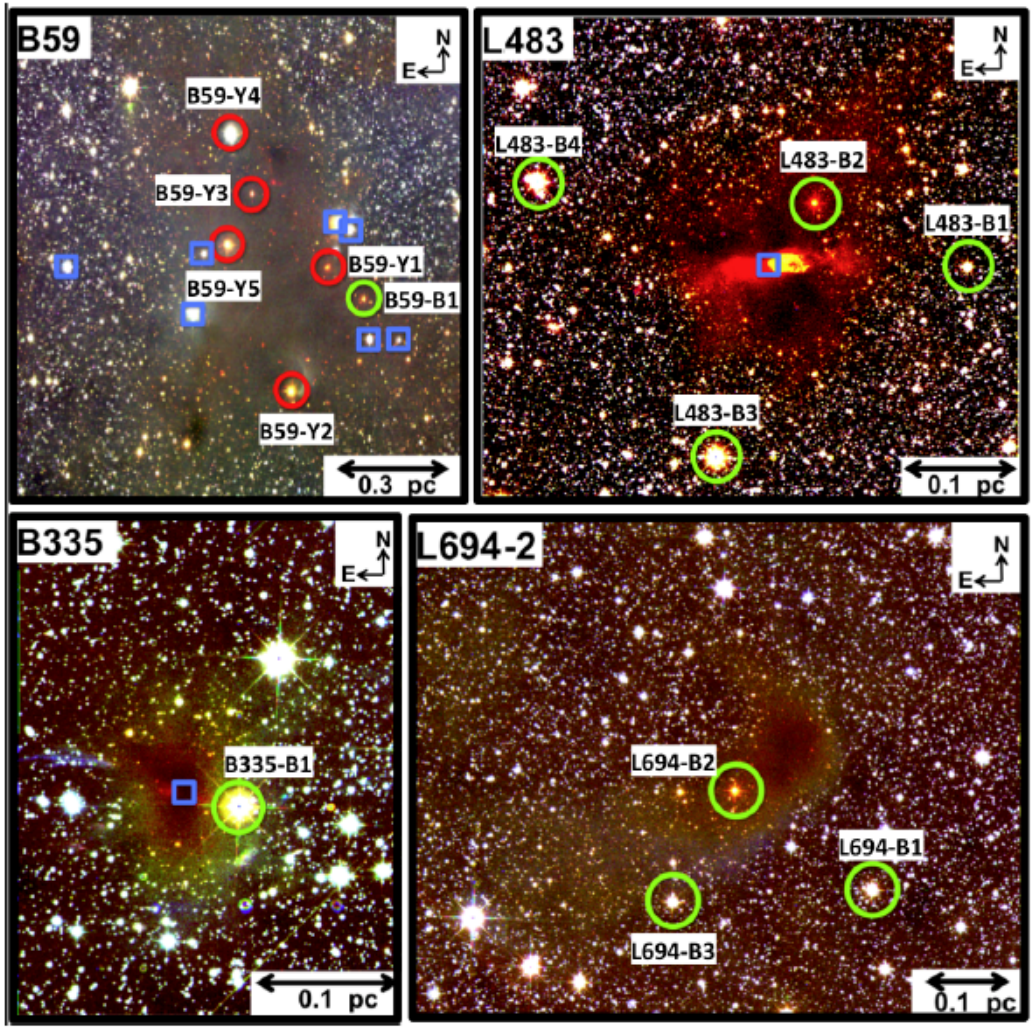

Figure 1. Color images for the molecular cores in which we study ice absorption features. These were made by combining JHK colors from the UKIRT WFCAM instrument. The following are the total exposure times used for each cloud: *B59*: J=1.0 hr, H=1.2 hr, K=1.4 hr, *L483*: J=5.6 hr, H=2.8 hr, K=2.8 hr, *B335*: J=4.0 hr, H=2.8 hr, K=3.2 hr. *L694-2*: J=3.2 hr, H=2.0 hr, K=2.0 hr. Stars circled in green represent background targets and red circles are YSO candidates in our sample. Blue squares show where other nearby YSOs are located in relation to targets in our sample. Size scales are shown for the quoted distances in the text for each core.

Chu+ 2020:

Observations of the Onset of Complex Organic Molecule Formation in Interstellar Ices

H_2O:3.0 um

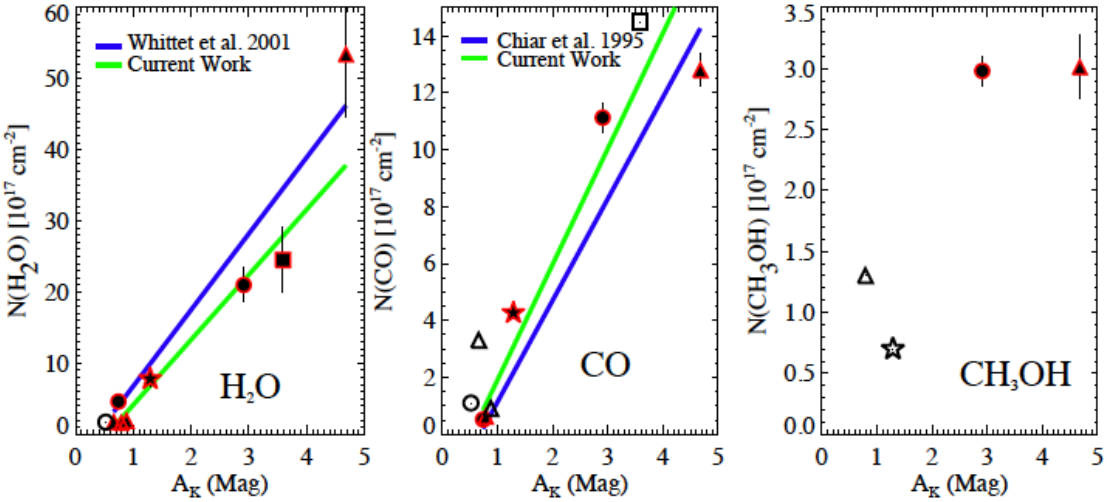

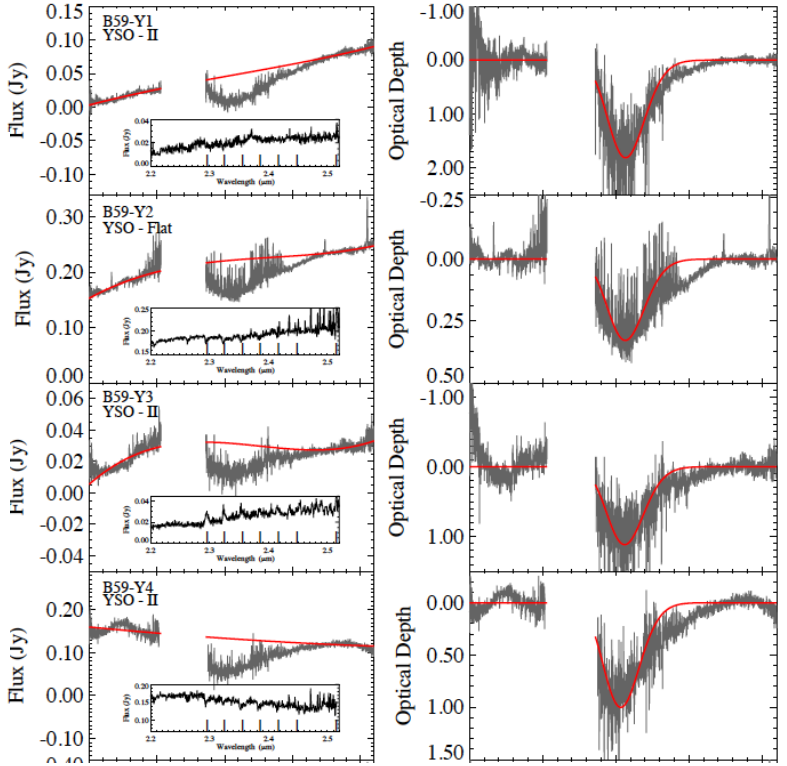

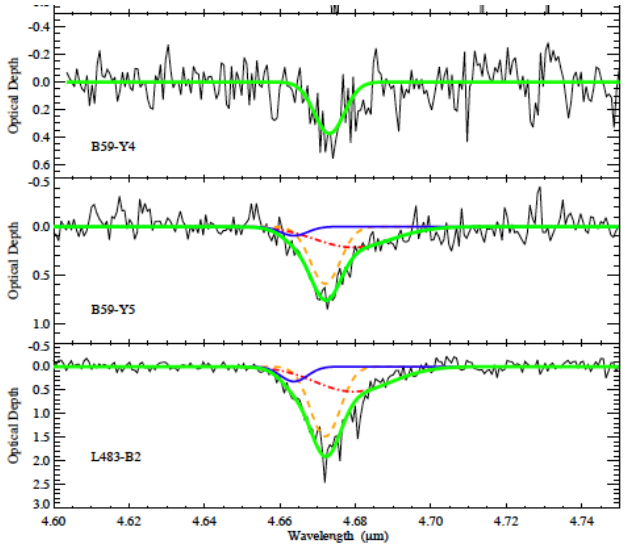

CO: 4.67 um

CH3OH
3.53 um

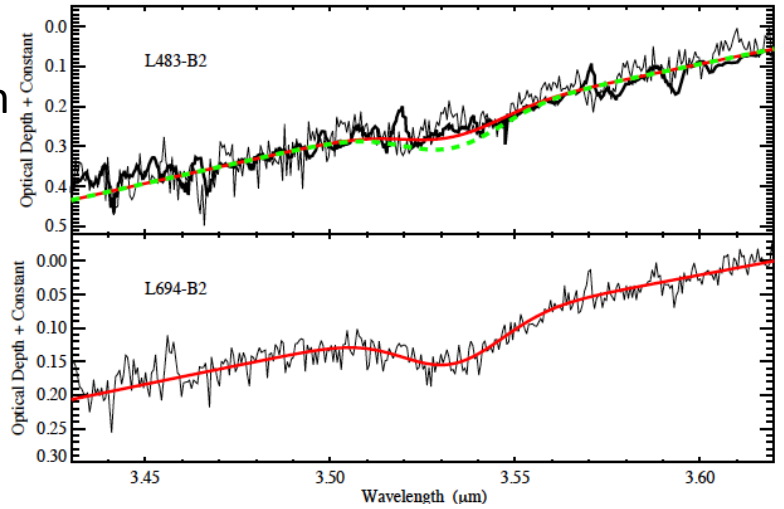

Chu+ 2021:

Constraining Spatial Densities of Early Ice Formation in Small Dense Molecular Cores form Extinction Maps

“NICER”(NIR Color Excess -> multiband) Equation

$$(J-H)^{obs} = (J-H)^{int} + 0.11 \times A_V$$
$$(H-K)^{obs} = (H-K)^{int} + 0.063 \times A_V$$
$$(K-[3.6])^{obs} = (K-[3.6])^{int} + 0.048 \times A_V$$
$$([3.6]-[4.5])^{obs} = ([3.6]-[4.5])^{int} + 0.015 \times A_V .$$

逆Abel変換したもの

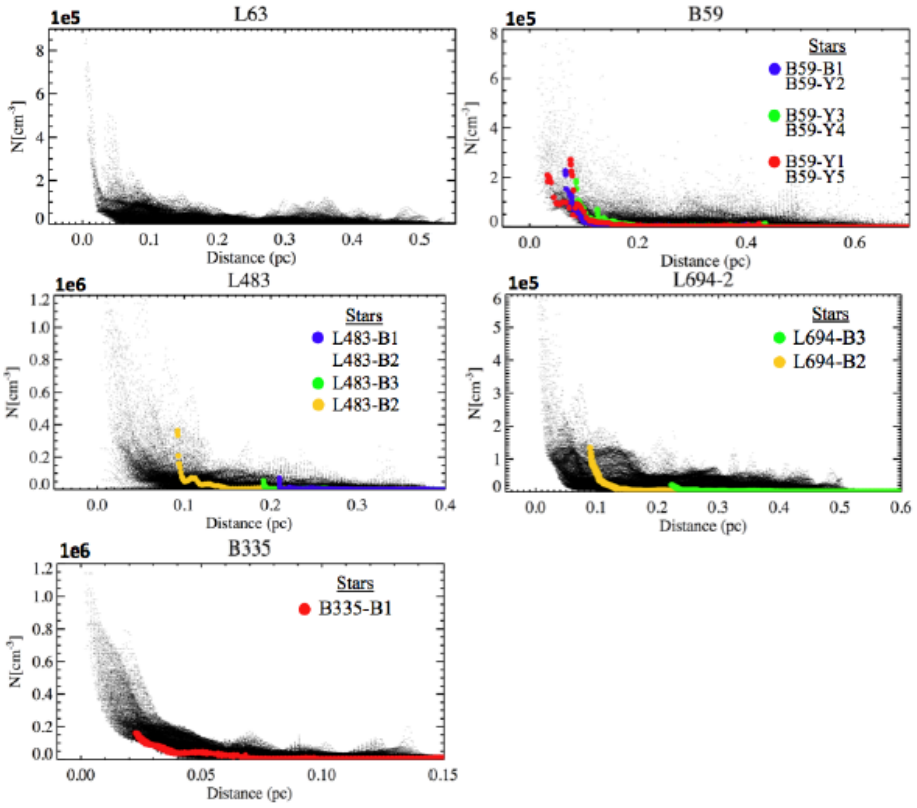

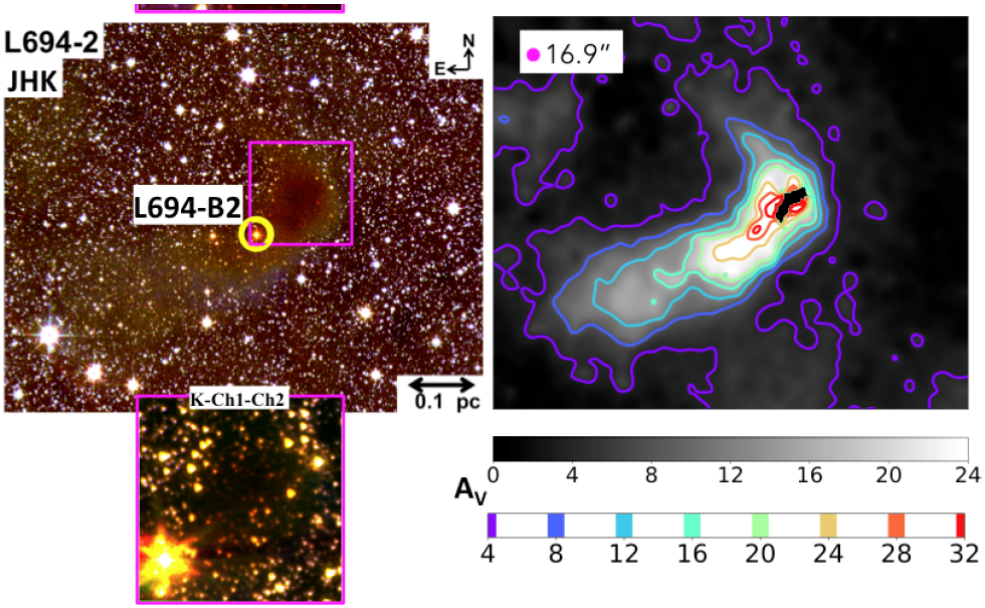

Background star

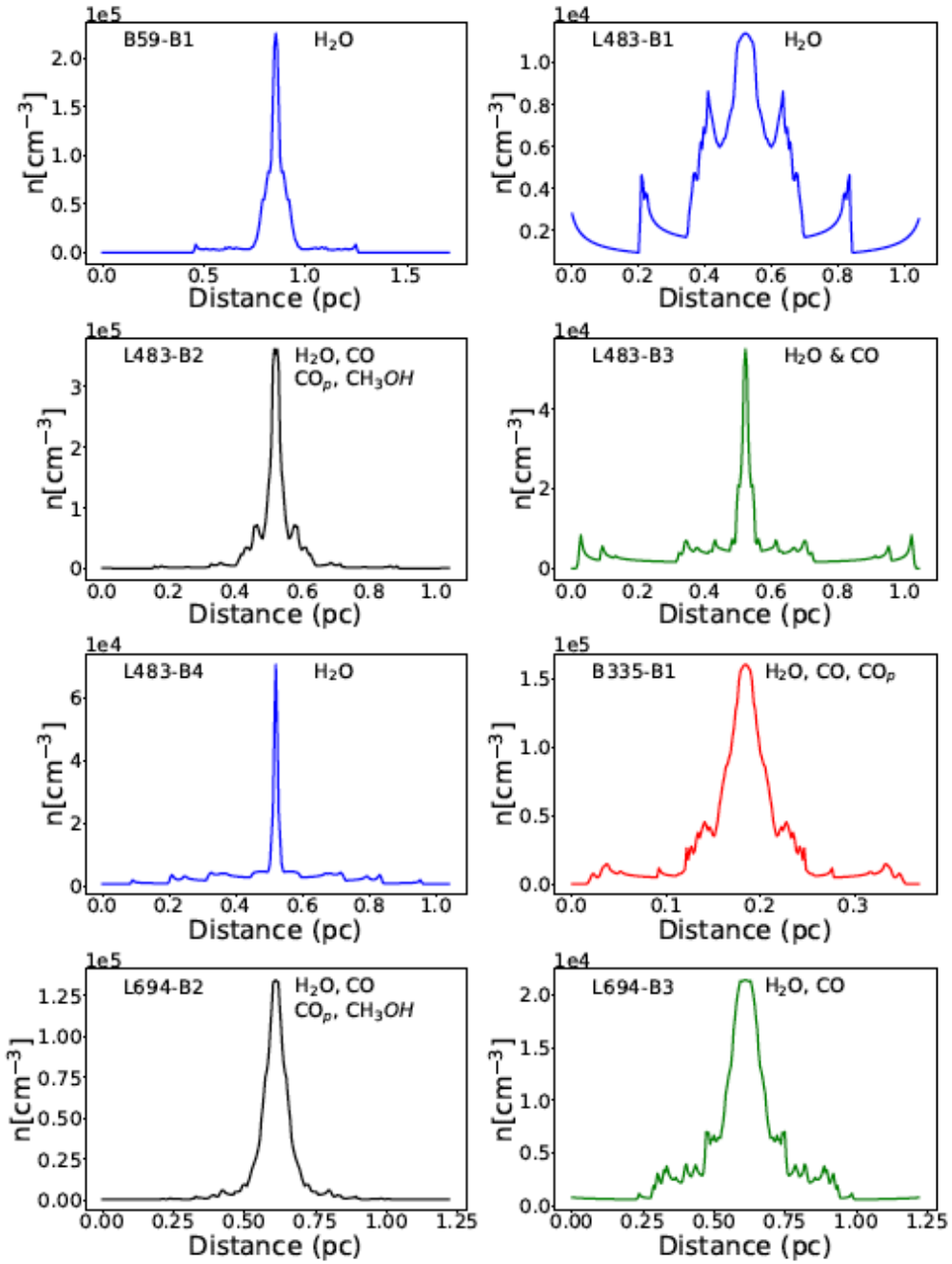

YSO

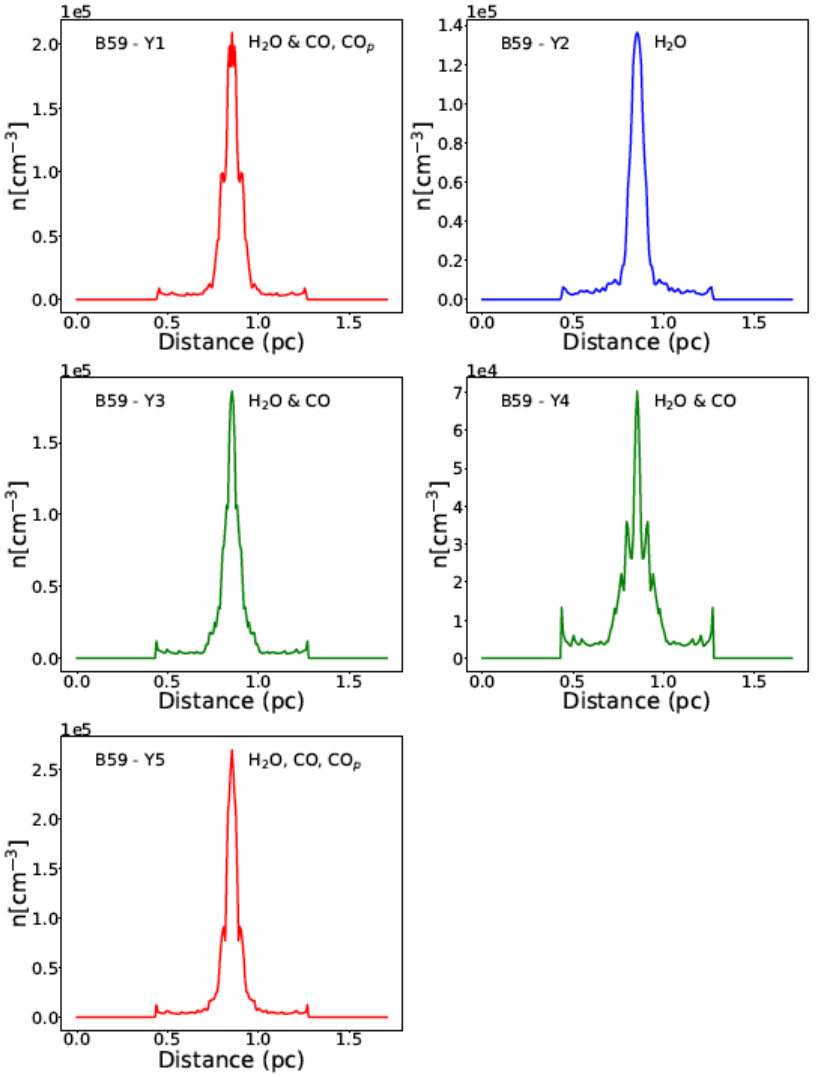

5. # TRAO Survey of the nearby filamentary molecular clouds, the universal nursery of stars (TRAO FUNS). II. Filaments and Dense cores in IC 5146

Eun Jung Chung, Chang Won Lee, Shinyoung Kim, Maheswar Gopinathan, Mario Tafalla, Paola Caselli, Philip C. Myers, Tie Liu, Hyunju Yoo, Kyoung Hee Kim, Mi-Ryang Kim, Archana Soam, Jungyeon Cho, Woojin Kwon, Changhoon Lee, Hyunwoo Kang

★ We present the results on the physical properties of filaments and dense cores in IC 5146, as a part of the TRAO FUNS project. We carried out On-The-Fly mapping observations using the Taeduk Radio Astronomy Observatory (TRAO) 14m telescope covering about 1 square degree of the area of IC 5146 using various molecular lines. We identified 14 filaments (24 in total, including sub-filaments) from the $C^{18}O$ (1-0) data cube and 22 dense cores from the N_2H^+ (1-0) data. We examined the filaments' gravitational criticality, turbulence properties, accretion rate from filaments to dense cores, and relative evolutionary stages of cores. Most filaments in IC 5146 are gravitationally supercritical within the uncertainty, and most dense cores are formed in them. We found that dense cores in the hubs show a systemic velocity shift of 0.3 km/s between the N_2H^+ and $C^{18}O$ gas. Besides, these cores are subsonic or transonic, while the surrounding filament gas is transonic or supersonic, indicating that the cores in the hubs are likely formed by the turbulence dissipation in the colliding turbulent filaments and the merging is still ongoing. We estimated the mass accretion rate of $15 - 35\ M_\odot\ \mathrm{Myr}^{-1}$ from the filaments to the dense cores, and the required time scales to collect the current core mass are consistent with the lifetime of the dense cores. The structures of filaments and dense cores in the hub can form by a collision of turbulent converging flows, and mass flow along the filaments to the dense cores may play an important role in forming dense cores.

IC516 (d ~600 - 800 pc)の分子輝線観測
TRAO 14m & 3-4 mm帯：H2H+, C18Oなど
- 分子ガスでのfilament, dense core同定
- filament は重力的super-critical

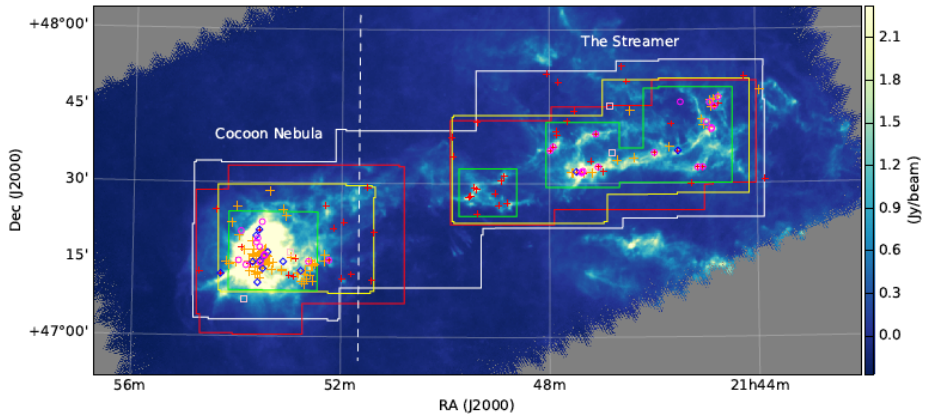

Figure 1. Our survey areas of IC 5146 marked over its *Herschel* 250 μm image. The areas observed in different molecular lines

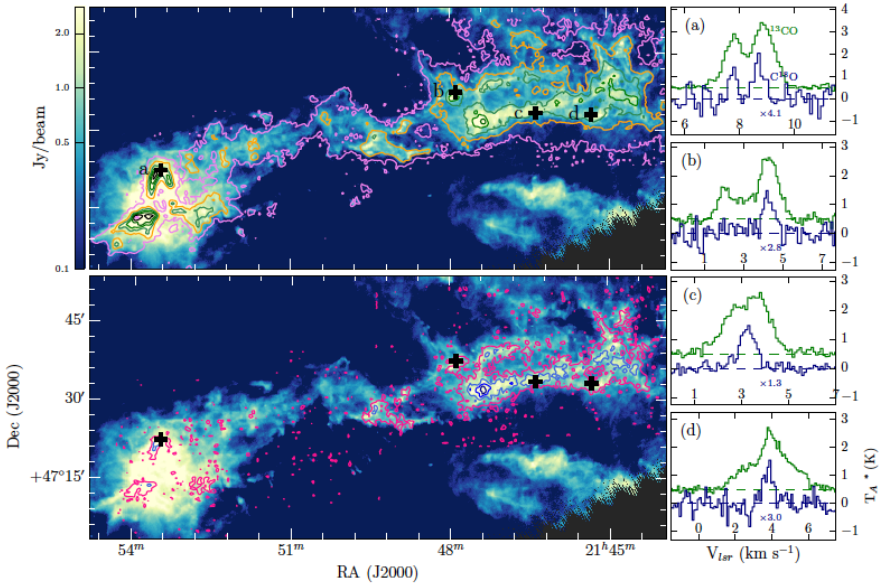

Figure 2. Integrated intensity maps of ^{13}CO (1 – 0) (top left) and $C^{18}O$ (1 – 0) (bottom left) with contours on the *Herschel* 250 μm image and spectra of the selected positions (right). The contour levels of ^{13}CO are 5, 20, 35, ⋯, 95×σ and those of $C^{18}O$ are 3, 8, 13, and 18×σ. The positions of the represented spectra in the right are indicated with crosses. In the right spectra panels, $C^{18}O$ line intensity is scaled up (the factor is written under each $C^{18}O$ spectrum).

6. **Probing jets from young embedded sources: clues from HST near-IR [Fe II] images**

Jessica Erkal, Brunella Nisini, Deirdre Coffey, Francesca Bacciotti, Patrick Hartigan, Simone Antoniucci, Teresa Giannini, Jochen Eislöffel, Carlo Felice Manara

★ We present near-infrared [Fe II] images of four Class 0/I jets (HH 1/2, HH 34, HH 111, HH 46/47) observed with the Hubble Space Telescope Wide Field Camera 3. The unprecedented angular resolution allows us to measure proper motions, jet widths and trajectories, and extinction along the jets. In all cases, we detect the counter-jet which was barely visible or invisible at shorter wavelengths. We measure tangential velocities of a few hundred km/s, consistent with previous HST measurements over 10 years ago. We measure the jet width as close as a few tens of au from the star, revealing high collimations of about 2 degrees for HH 1, HH 34, HH 111 and about 8 degrees for HH 46, all of which are preserved up to large distances. For HH 34, we find evidence of a larger initial opening angle of about 7 degrees. Measurement of knot positions reveals deviations in trajectory of both the jet and counter-jet of all sources. Analysis of asymmetries in the inner knot positions for HH 111 suggests the presence of a low mass stellar companion at separation 20-30 au. Finally, we find extinction values of 15-20 mag near the source which gradually decreases moving downstream along the jet. These observations have allowed us to study the counter-jet at unprecedented high angular resolution, and will be a valuable reference for planning future JWST mid-infrared observations which will peer even closer into the jet engine.

HST Wide Field Camera 3で　NIR [Fe II] 輝線観測を実施

4つの Class0/I jets; HH1/2, HH34, HH111, HH46/47

高空間分解能で、proper motion, jet width, jetの軌跡などを調べた

結果

- jet width (星から20-30 au): collimation ~ 2 deg. (HH1, HH34, HH111), & 8 deg. (HH46)
- jet trajectory のasymmetry がjet＆counter-jet両方で見られる(全天体)
- Jet asymmetry (HH111) => wiggle的で、a low mass stellar companion at 20-30 auが存在?

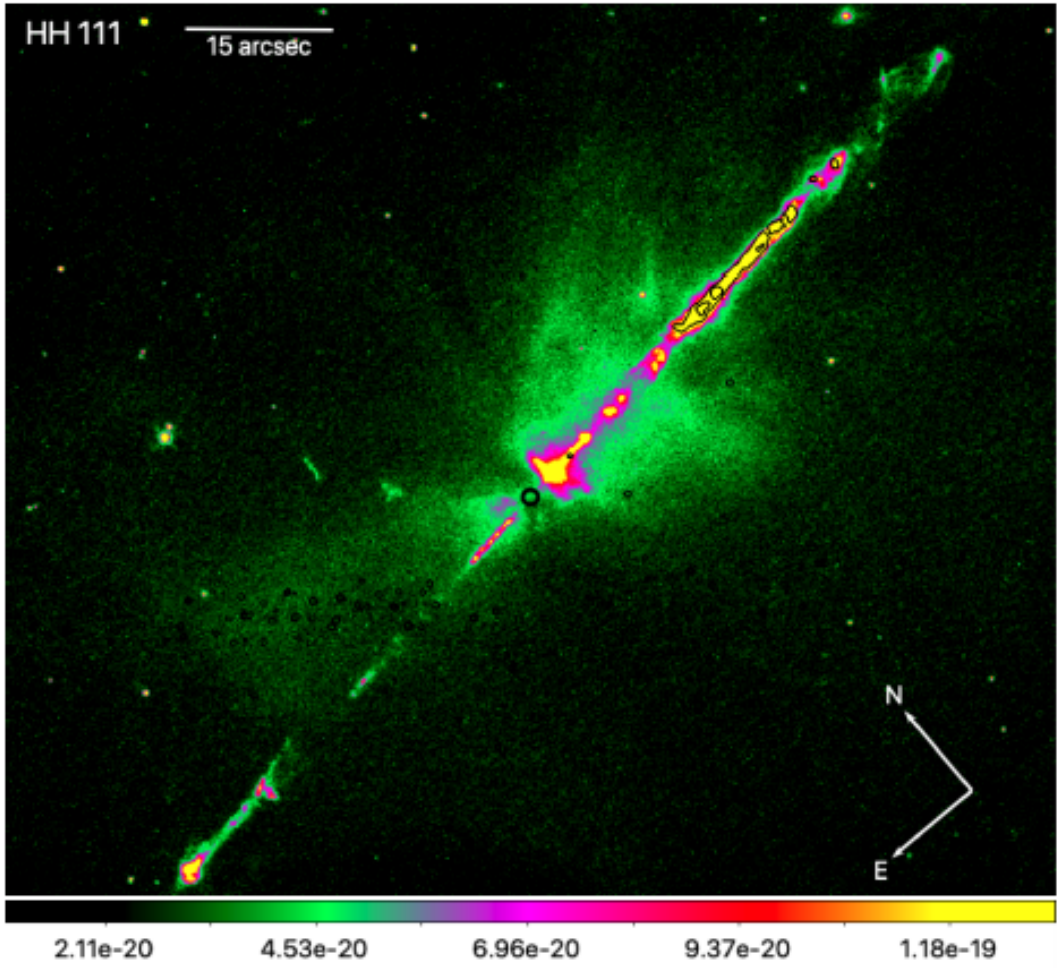

Figure 5. [Fe II] 1.64μm line+continuum image of the HH 111 jet and cavity. [O I] contours are overplotted in black (levels are 0.2 and 1 $\times 10^{-19}$ **erg s^{-1} cm^{-2} Å^{-1} pixel^{-1}**), showing that at optical wavelengths the jet is observed only at large distances from the source (marked by the black circle). The red-shifted jet is not detected in the optical.

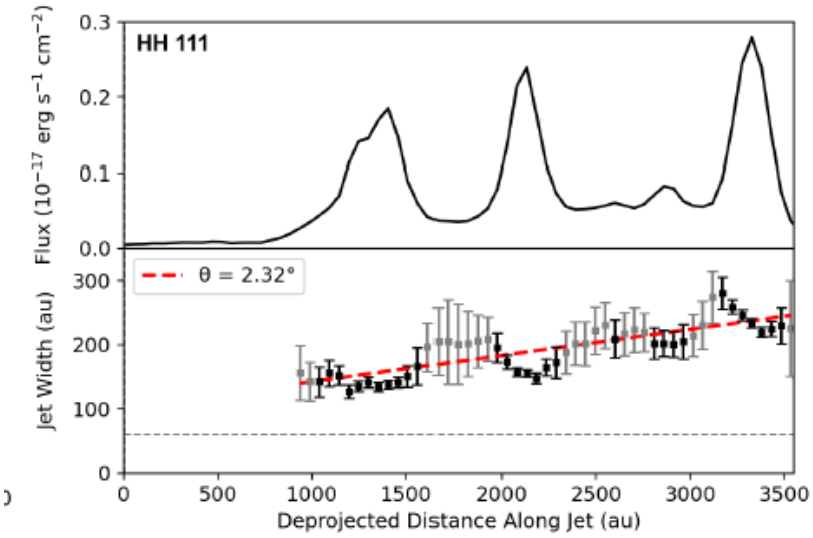

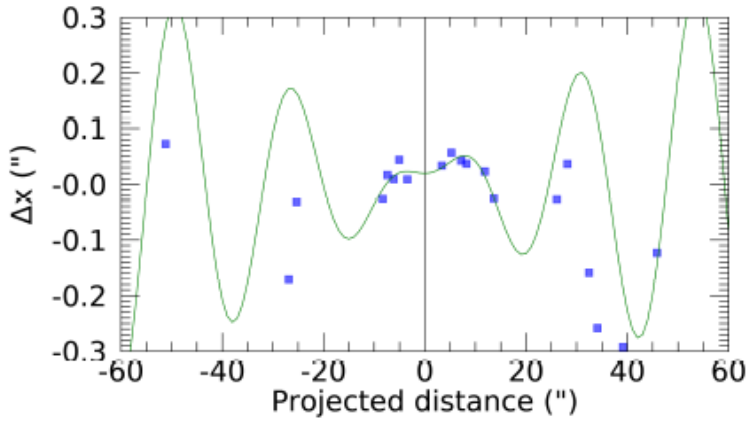

Figure 17. A model fit to the observed photocentre offse positions of the HH 111 inner knots as a function of distanc from the exciting source. Blue boxes indicate the measure offsets. The solid green line is the best fit of the interna knots wiggle produced by an orbital motion of the jet sourc around a companion.